Explicit theoretical analysis of how the rate of exocytosis depends on local control by Ca^{2+} channels

Francesco Montefusco [*1] and Morten Gram Pedersen[*1,2,3]

[1]Department of Information Engineering, University of Padova, Padova, Italy
[2]Department of Mathematics "Tullio Levi-Civita", University of Padova, Padova, Italy
[3]Padova Neuroscience Center, University of Padova, Padova, Italy

Abstract

Hormones and neurotransmitters are released from cells by calcium-regulated exocytosis, and local coupling between Ca^{2+} channels (CaVs) and secretory granules is a key factor determining the exocytosis rate. Here, we devise a methodology based on Markov chain models that allows us to obtain analytic results for the expected rate. First, we analyze the property of the secretory complex obtained by coupling a single granule with one CaV. Then, we extend our results to a more general case where the granule is coupled with n CaVs. We investigate how the exocytosis rate is affected by varying the location of granules and CaVs. Moreover, we assume that the single granule can form complexes with inactivating or non-inactivating CaVs. We find that increasing the number of CaVs coupled with the granule determines a much higher rise of the exocytosis rate that, in case of inactivating CaVs, is more pronounced when the granule is close to CaVs, while, surprisingly, in case of non-inactivating CaVs, the highest relative increase in rate is obtained when the granule is far from the CaVs. Finally, we exploit the devised model to investigate the relation between exocytosis and calcium influx. We find that the quantities are typically linearly related, as observed experimentally. For the case of inactivating CaVs, our simulations show a change of the linear relation due to near-complete inactivation of CaVs.

Introduction

Molecules, e.g. neurotransmitters and proteins, are released from the cell by exocytosis [1]. In this paper we focus on regulated exocytosis in the endocrine cells that release different kind of hormones regulating various physiological processes [2]. When hormone secretion is defectively regulated, several diseases may develop. For example, in diabetes, the two main pancreatic hormones, insulin and glucagon, are not released appropriately for fine-tuning glucose homeostasis [3, 4]. Therefore it is crucial to achieve a better understanding

[*]montefusco@dei.unipd.it; pedersen@dei.unipd.it

of the main mechanisms underlying hormone exocytosis that determines the control of different physiological processes.

In most endocrine cells, the hormones are contained in secretory granules that, in response to a series of cellular mechanisms culminating with an increase in the intracellular Ca^{2+} levels, fuse with the cell membrane and release the hormone molecules. The main mechanisms regulating hormone exocytosis are shared with exocytosis of synaptic vesicles underlying neurotransmitter release in neurons [1, 5]. The granules contain v-SNARE proteins that can form the so-called SNARE complexes with t-SNAREs inserted in the cell membrane [1]. SNARE complexes interact with other proteins, notably Ca^{2+}-sensing proteins such as synaptotagmins, which trigger exocytosis upon Ca^{2+} binding. Therefore, the local Ca^{2+} concentration at the Ca^{2+} sensor of the exocytotic machinery is a key factor determining the probability (rate) of exocytosis of the secretory granule.

Recently, we have devised a detailed model of Ca^{2+} dynamics and exocytosis for the glucagon-secreting pancreatic alpha-cells, and showed how exocytosis is dependent on calcium dynamics, in particular, on calcium levels surrounding the Ca^{2+} channels (CaVs) [6], the so-called nanodomains [7]. Here, in order to characterize the local interactions between the single granule and the surrounding CaVs, we will exploit a strategy that is similar to the methodology devised in our recent paper to describe the large conductance BK potassium current that is controlled locally by CaVs [8]. We showed that the number and the type of CaVs coupled with the BK channel affect the electrical activity of neurons and other excitable cells, such as pancreatic beta-cells and pituitary cells. Therefore, we will implement mathematical modelling for characterizing the local interactions between granules and CaVs and, specifically, Markov chain models that could provide important insight into the exocytosis rate. In particular, by using the Markov chain theory [9], we will achieve analytic results for the expected rate, and show how coupling different numbers and types of CaVs with the granule determines different responses.

Methods

CaV channel model

We model the Ca^{2+} channel by using the 3-state Markov chain of Fig. 1A, where C corresponds to the closed state, O to the open state and B to the inactivated (blocked) state of the calcium channel [10]. Then, the CaV model takes values in the state space $S = \{C, O, B\}$ and its transition rate or generator matrix M_{CaV} is given by

$$M_{CaV} = \begin{bmatrix} -\alpha & \alpha & 0 \\ \beta & -\beta - \delta & \delta \\ 0 & \gamma & -\gamma \end{bmatrix}. \tag{1}$$

Here, α and β represent the voltage-dependent Ca^{2+} channel opening rate and closing rate, respectively, and have the following forms:

$$\alpha(V) = \alpha_0 e^{-\alpha_1 V}, \tag{2}$$

$$\beta(V) = \beta_0 e^{-\beta_1 V}. \tag{3}$$

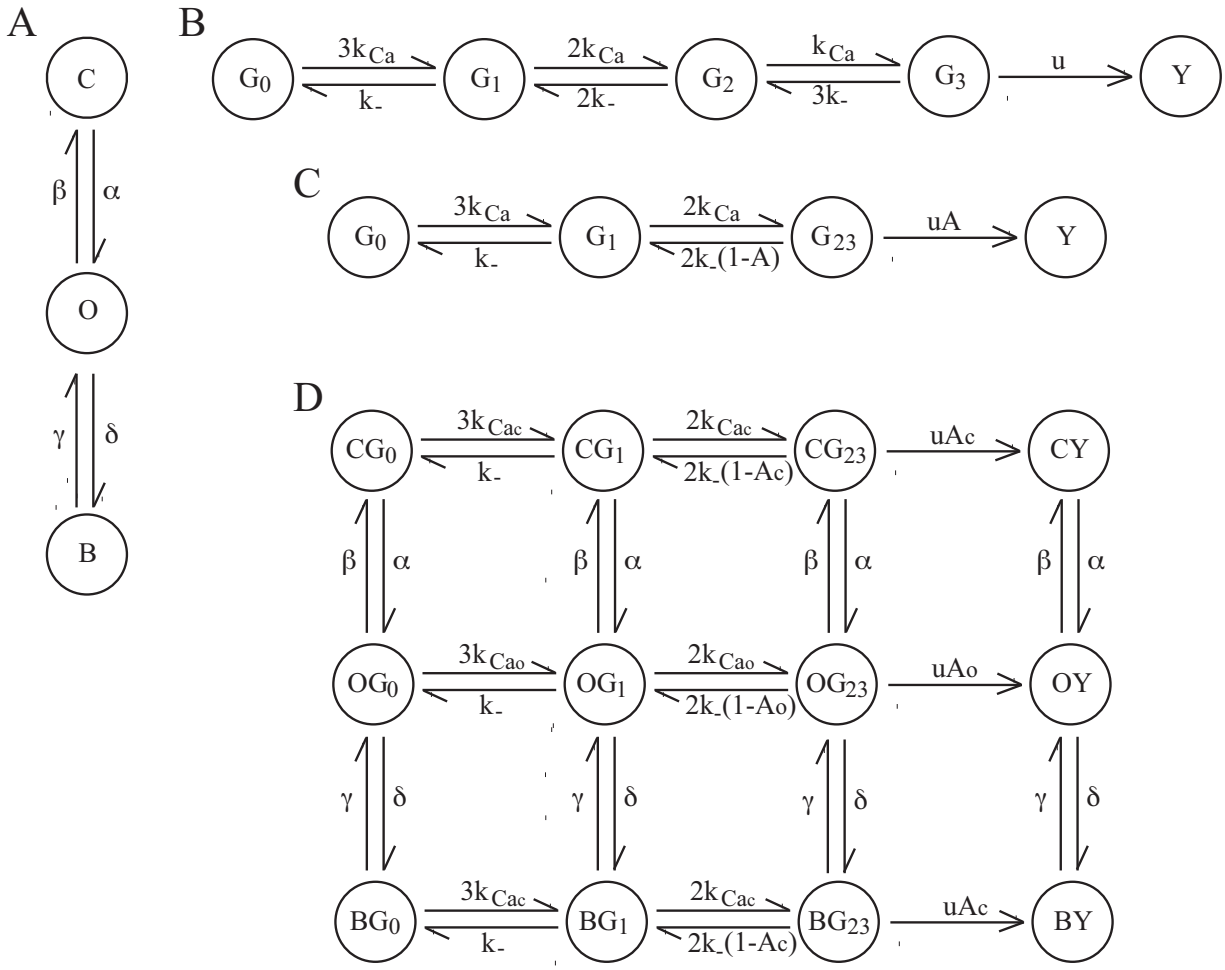

Figure 1: **Markov chain models for Ca^{2+} channel (CaV), exocytosis of single granule and granule-CaV complex**. **(A)** Markov chain model for CaV, where C is the closed state, O the open state and B the inactivated or blocked state. **(B)** Markov chain model for exocytosis of a single granule adjacent to the plasma membrane, where G_0 correspond to the state with no bound Ca^{2+} ions, G_1 with one, G_2 with two, and G_3 with three. **(C)** Markov chain model for the approximated exocytosis model where the dynamics of states G_2 and G_3 are described by the auxiliary variable G_{23} using quasi-steady state approximation for the corresponding ODE model. **(D)** Markov chain model for the granule-CaV complex where the granule dynamics are described by the model shown in panel (C) and the CaV dynamics by the model shown in panel (A).

The rate for channel inactivation, δ, is Ca^{2+}-dependent, and has the following form

$$\delta = \delta_0 \times [Ca_{CaV}]\,. \tag{4}$$

Ca_{CaV} is the Ca^{2+} concentration at the Ca^{2+} sensor for inactivation, and is given using reaction-diffusion theory [7, 11, 12] by

$$Ca_{CaV} = \frac{i_{Ca_{max}}}{8\pi r_{Ca} D_{Ca} F} \exp\left[\frac{-r_{Ca}}{\sqrt{\frac{D_{Ca}}{k_B^+[B_{total}]}}}\right], \tag{5}$$

where $i_{Ca_{max}} = \bar{g}_{Ca}(V - V_{Ca})$ is the single-channel Ca^{2+} current with $\bar{g}_{Ca}$ the single-channel conductance and V_{Ca} the reverse potential, and r_{Ca} represents the distance of the sensor for Ca^{2+}-dependent inactivation from the channel pore. Finally, γ is the constant reverse reactivation rate. Table 1 reports the parameter values for the CaV model defined by above equations.

The deterministic description of the 3-state Markov Chain model for the CaV channel is given by the following ODE system

$$\frac{dc}{dt} = \beta o - \alpha c, \tag{6}$$

$$\frac{do}{dt} = \alpha c + \gamma b - (\beta + \delta) o, \tag{7}$$

$$b = 1 - c - o = 1 - h, \tag{8}$$

where the italic lowercase letters represent the corresponding state variables of the ODE model (h represents the fraction of Ca^{2+} channels not inactivated).

Finally, in order to investigate the relationship between exocytosis and Ca^{2+} loading, we compute the total charge entering via the Ca^{2+} channel at a given step voltage with time window, t_s, as

$$Q_{Ca} = \int_0^{t_s} o\,(\tau) \cdot i_{Ca_{max}} d\tau. \tag{9}$$

Exocytosis model

We assume a single granule, adjacent to the plasma membrane and primed for exocytosis, that can be in one of four different states depending on the number of Ca^{2+} ions bound to the Ca^{2+} sensor on the granule, likely synaptotagmin [13]: in G_0 with no bound Ca^{2+} ions, or in G_1 with one, or in G_2 with two, or in G_3 with three bound ions. Once it is in G_3, the granule can fuse with the membrane and release its hormone content, assuming the final state Y [14, 15]. Therefore, we use a five-state Markov chain model for describing exocytosis as shown in Fig. 1B, where the model takes values in the state space

Table 1: **Model parameters**

CaV model parameters		
Parameter	Value	Unit
α_0	0.6	ms^{-1}
α_1	-0.1	mV^{-1}
β_0	0.2	ms^{-1}
β_1	0.0375	mV^{-1}
γ	0.002	ms^{-1}
δ_0	0.0025	$\mu\mathrm{M}^{-1}\ \mathrm{ms}^{-1}$
Parameters for calculating Ca^{2+} concentration at different distances		
Parameter	Value	Unit
r_{Ca}	7	nm
r_G	10, 20, 30, 50	nm
D_{Ca}	250	$\mu\mathrm{m}^2\ \mathrm{s}^{-1}$
F	9.6485	$\mathrm{C\ mol}^{-1}$
k_B	500	$\mu\mathrm{M}^{-1}\ \mathrm{s}^{-1}$
B_{total}	30	μM
V_{Ca}	60	mV
$\bar{g}_{Ca}$	2.8	pS
Ca_c	0.1	μM
Ca_b	0.1	μM
Exocytosis model parameters		
Parameter	Value	Unit
k_{Ca}	1.85	$\mu\mathrm{M}^{-1}\ \mathrm{s}^{-1}$
k_-	50	s^{-1}
u	1000	s^{-1}

$S = \{G_0, G_1, G_2, G_3, Y\}$ and its transition rate or generator matrix M_G is given by

$$M_G = \begin{bmatrix} -3\,k_{Ca} & 3\,k_{Ca} & 0 & 0 & 0 \\ k_- & -2\,k_{Ca} - k_- & 2\,k_{Ca} & 0 & 0 \\ 0 & 2\,k_- & -k_{Ca} - 2\,k_- & k_{Ca} & 0 \\ 0 & 0 & 3\,k_- & -u - 3\,k_- & u \\ 0 & 0 & 0 & 0 & 0 \end{bmatrix}. \tag{10}$$

where

$$k_{Ca} = k \times [Ca_G] \tag{11}$$

represents the Ca^{2+} binding rate with Ca_G the Ca^{2+} concentration at the granule sensor given by equation (5) with $r = r_G$ being the distance from the CaV to the Ca^{2+} sensor on the granule. In the following, the distance from the CaV to the granule means the distance from the CaV to the Ca^{2+} sensor on the granule, which will be of the order of tens of nm. For comparison, secretory granules have diameters on the order 100-500 nm [16, 17, 18, 19]. We assume a constant number of Ca^{2+} sensor molecules, which is therefore

included in the binding parameter k_{Ca}. The parameter k_- is the unbinding rate, and u is the fusion rate. Table 1 reports the parameter values.

The deterministic description of the 5-state Markov Chain model for exocytosis is given by the following ODE system

$$\frac{dg_0}{dt} = -3\,k_{Ca}g_0 + k_-g_1, \tag{12}$$

$$\frac{dg_1}{dt} = -(2\,k_{Ca} + k_-)g_1 + 3\,k_{Ca}g_0 + 2\,k_-g_2, \tag{13}$$

$$\frac{dg_2}{dt} = -(k_{Ca} + 2\,k_-)g_2 + 2\,k_{Ca}g_1 + 3\,k_-g_3, \tag{14}$$

$$\frac{dg_3}{dt} = -(u + 3\,k_-)g_3 + k_{Ca}g_2, \tag{15}$$

$$y = 1 - g_0 - g_1 - g_2 - g_3\,. \tag{16}$$

For the above ODE model of equations (12)–(16), we exploit quasi steady-state approximation for state g_3, since its dynamics are fastest (the value of u is much higher than those of the other parameters). Then, by renaming the state variables as

$$g_{23} = g_2 + g_3\,, \tag{17}$$

by setting equation (15) equal to zero yielding

$$g_3 = A\,g_{23}\,,\ \text{with}\ \ A = \frac{k_{Ca}}{k_{Ca} + 3\,k_- + u}\,, \tag{18}$$

and by summing equations (14)-(15), we achieve a single ODE model for describing the dynamics of state variable g_2 and g_3 as follows:

$$\frac{dg_{23}}{dt} = -\left(2\,k_-\,(1 - A) + u\,A\right)g_{23} + 2\,k_{Ca}g_1\,. \tag{19}$$

The corresponding Markov chain model takes values in the state space $S = \{G_0, G_1, G_{23}, Y\}$ (see Fig. 1C) and is described by the following generating matrix, $M_{G_{ap}}$:

$$M_{G_{ap}} = \begin{bmatrix} -3\,k_{Ca} & 3\,k_{Ca} & 0 & 0 \\ k_- & -2\,k_{Ca} - k_- & 2\,k_{Ca} & 0 \\ 0 & 2\,k_-\,(1 - A) & -2\,k_-\,(1 - A) - u\,A & u\,A \\ 0 & 0 & 0 & 0 \end{bmatrix}. \tag{20}$$

Note that state Y of the Markov chain described by $M_{G_{ap}}$ is an absorbing state: the process can never leave Y after entering it, reflecting that fusion is an irreversible process. Then $M_{G_{ap}}$ can be rewritten as

$$M_{G_{ap}} = \begin{bmatrix} D_{3\times3} & \mathbf{d}_{3\times1} \\ \mathbf{0}_{1\times3} & 0 \end{bmatrix}. \tag{21}$$

where

$$D_{3\times3} = \begin{bmatrix} -3\,k_{Ca} & 3\,k_{Ca} & 0 \\ k_- & -2\,k_{Ca} - k_- & 2\,k_{Ca} \\ 0 & 2\,k_-\,(1-A) & -2\,k_-\,(1-A) - u\,A \end{bmatrix} \tag{22}$$

describes only the transitions between the transient states G_0, G_1 and G_{23}, and $\mathbf{d} = [0\,,0\,,u\,A]^\intercal$ is a vector containing the transition intensities from the transient states to the absorbing state Y. The row vector $\mathbf{0} \in \mathbb{R}^{1\times3}$ consists entirely of 0's since no transitions from Y to the transient states can occur. The remaining element of the matrix $M_{G_{ap}}$ is 0 and gives the transition rate out of the absorbing state.

Using phase-type distribution results for Markov chains [9], we obtain an explicit formula for calculating the expected event rate λ_Y to reach the absorbing state Y, given the initial probability row vector $\boldsymbol{\pi}$ for the transient states ($\boldsymbol{\pi} = (\pi_{G_0}, \pi_{G_1}, \pi_{G_{23}})$), as

$$\lambda_Y = \frac{1}{\boldsymbol{\pi}\,(-D^{-1})\,\mathbf{1}} \tag{23}$$

where $\mathbf{1} \in \mathbb{R}^{3\times1}$.

Granule-CaV complex model with 1:1 and 1:n stoichiometries

1:1 stoichiometry

By coupling the CaV and exocytosis models, we obtain the 12-state Markov chain model of Fig. 1D. The model takes values in the state space

$$S = \{CG_0, OG_0, BG_0, CG_1, OG_1, BG_1, CG_{23}, OG_{23}, BG_{23}, CY, OY, BY\},$$

and its transition matrix, $D_{G:CaV}$, is as follows:

$$D_{G:CaV_{9\times9}} = \begin{bmatrix} M_{CaV} - 3\,\mathrm{diag}\,(k_{Ca_c}, k_{Ca_o}, k_{Ca_c}) & 3\,\mathrm{diag}\,(k_{Ca_c}, k_{Ca_o}, k_{Ca_c}) & \mathbf{0}_{3\times3} \\ \mathrm{diag}\,(k_-, k_-, k_-) & M_{CaV} - \mathrm{diag}\,(2k_{Ca_c} + k_-, 2k_{Ca_o} + k_-, 2k_{Ca_c} + k_-) & 2\,\mathrm{diag}\,(k_{Ca_c}, k_{Ca_o}, k_{Ca_c}) \\ \mathbf{0}_{3\times3} & 2\,k_-\,\mathrm{diag}\,((1-A_c)\,,(1-A_o)\,,(1-A_c)) & M_{CaV} - \mathrm{diag}\,(2\,k_-\,(1-A_c) + u\,A_c, 2\,k_-\,(1-A_o) + u\,A_o, 2\,k_-\,(1-A_c) + u\,A_c) \end{bmatrix} \tag{24}$$

where M_{CaV} is defined by equation (1), k_{Ca_c} (A_c) by equation (11) (equation (18)) with $Ca_G = Ca_c$, i.e. the concentration at the granule when the associated CaV is closed (or inactivated, i.e. $Ca_c = Ca_b$), and k_{Ca_o} (A_o) by equation (11) (equation (18)) with $Ca_G = Ca_o$, i.e., the concentration at the granule when the associated CaV is open, computed by equation (5). Then, the expected exocytosis rate for the single granule, λ_{Y_1}, can be estimated by using equation (23), assuming initially the granule in state G_0 and the CaV closed, i.e the complex in the state CG_0 ($\boldsymbol{\pi} = (1, \mathbf{0}_{1\times8})$), as

$$\lambda_{Y_1} = \frac{1}{\boldsymbol{\pi}\left(-{D_{G:CaV}}^{-1}\right)\mathbf{1}} \tag{25}$$

where $\mathbf{1} \in \mathbb{R}^{9\times1}$.

We also consider the particular case with non-inactivating CaV (i.e. the Ca^{2+} channel can be only in C or in O). In this case, $M_{CaV} \in \mathbb{R}^{2\times2}$ and is defined by equation (1) with $\delta = \gamma = 0$, and then $D_{G:CaV}$, given by equation (24), belongs to $\mathbb{R}^{6\times6}$.

1:n stoichiometry

In the following, we assume the case where the granule is coupled with more than one CaV. In particular, by considering k Ca^{2+} channels, we have a Markov chain model with $n_S = \sum_{i=0}^{k} (k+1-i) = \frac{k^2}{2} + \frac{3k}{2} + 1$ possible states describing the k CaVs. In particular, the CaVs model takes values in the state space $S = \{C_{k-i-j} O_i B_j\}$ with $j \in \{0, \dots, k\}$ and $i \in \{0, \dots, k-j\}$, and its generating matrix, M_{kCaV}, is given by

$$M_{kCaV_{n_S \times n_S}} = \begin{bmatrix} M_{0_{(k+1)\times(k+1)}} & \mathbf{0}_{1\times k} & 0 & \cdots & \cdots & \cdots & \cdots & \cdots & 0 \\ & \delta \operatorname{diag}(1, \dots, k) & & & & & & & \\ \mathbf{0}_{k\times 1} & \gamma I_k & \ddots & \ddots & 0 & \cdots & \cdots & \cdots & \vdots \\ 0 & & \ddots & \ddots & \ddots & 0 & \cdots & \cdots & \vdots \\ \vdots & & \cdots & 0 & \mathbf{0}_{(k+1-j)\times 1} & j\,\gamma I_{(k+1-j)} & M_{j_{(k+1-j)\times(k+1-j)}} & \mathbf{0}_{1\times(k-j)} & 0 & \cdots & \vdots \\ & & & & & & & \delta \operatorname{diag}(1, \dots, k-j) & & & \\ \vdots & & \cdots & \cdots & \cdots & 0 & \ddots & \ddots & \ddots & 0 \\ \vdots & & \cdots & \cdots & \cdots & \cdots & 0 & \ddots & \ddots & \delta \\ \vdots & & \cdots & \cdots & \cdots & \cdots & \cdots & 0 & k\gamma & M_{k_{1\times 1}} \end{bmatrix} \tag{26}$$

where

$$M_{0_{(k+1)\times(k+1)}} = \begin{bmatrix} -k\alpha & k\alpha & 0 & \cdots & \cdots & \cdots & \cdots & \cdots & 0 \\ \beta & \ddots & \ddots & 0 & \cdots & \cdots & \cdots & \cdots & \vdots \\ 0 & \ddots & \ddots & \ddots & 0 & \cdots & \cdots & \cdots & \vdots \\ \vdots & \cdots & 0 & (i-1)\beta & -(k-(i-1))\,\alpha - (i-1)\,(\beta+\delta) & (k-(i-1))\,\alpha & 0 & \cdots & \vdots \\ \vdots & \cdots & \cdots & \cdots & 0 & \ddots & \ddots & \ddots & 0 \\ \vdots & \cdots & \cdots & \cdots & \cdots & 0 & \ddots & \ddots & \alpha \\ 0 & \cdots & \cdots & \cdots & \cdots & \cdots & 0 & k\beta & -k\,(\beta+\delta) \end{bmatrix}, \tag{27}$$

and

$$M_{j_{(k+1-j)\times(k+1-j)}} = \begin{bmatrix} -(k-j)\,\alpha - j\gamma & (k-j)\,\alpha & 0 & \cdots & \cdots & \cdots & \cdots & \cdots & 0 \\ \beta & \ddots & \ddots & 0 & \cdots & \cdots & \cdots & \cdots & \vdots \\ 0 & \ddots & \ddots & \ddots & 0 & \cdots & \cdots & \cdots & \vdots \\ \vdots & \cdots & 0 & (i-1)\beta & -(k-(i-1)-j)\,\alpha - (i-1)\,(\beta+\delta) - j\gamma & (k-(i-1)-j)\,\alpha & 0 & \cdots & \vdots \\ \vdots & \cdots & \cdots & \cdots & 0 & \ddots & \ddots & \ddots & 0 \\ \vdots & \cdots & \cdots & \cdots & \cdots & 0 & \ddots & \ddots & \alpha \\ 0 & \cdots & \cdots & \cdots & \cdots & \cdots & 0 & (k-j)\,\beta & -(k-j)\,(\beta+\delta) - j\gamma \end{bmatrix}. \tag{28}$$

and $M_{k_{1\times 1}} = -k\gamma$.

Then, by coupling the CaVs and exocytosis models, we obtain a $4n_S$-state Markov chain model. The model takes values in the state space $S = \{C_{k-i-j} O_i B_j G_l, \dots, C_{k-i-j} O_i B_j G_{23}, C_{k-i-j} O_i B_j Y\}$, with $j \in \{0, \dots, k\}$, $i \in \{0, \dots, k-j\}$ and $l \in \{0, 1\}$, and its transition matrix, $D_{G:kCaV}$, can be written as

$$D_{G:kCaV_{3n_S\times 3n_S}} = \begin{bmatrix} M_{kCaV} - K_{Ca_1} & K_{Ca_1} & \mathbf{0}_{n_S\times n_S} \\ k_-\, I_{n_S} & M_{kCaV} - K_{Ca_2} - k_-\, I_{n_S} & K_{Ca_2} \\ \mathbf{0}_{n_S\times n_S} & 2\,k_-\,(I_{n_S} - D_A) & M_{kCaV} - 2\,k_-\,(I_{n_S} - D_A) - u\,D_A \end{bmatrix} \tag{29}$$

where

$$K_{Ca_{1_{n_S\times n_S}}} = \begin{bmatrix} 3\,k_{Ca_c} & 0 & & & & & \\ 0 & 3\,k_{Ca_o}\,\mathrm{diag}\,(1,\ldots,k) & & & & & \\ & & \ddots & & & & \\ & & & 3\,k_{Ca_c} & 0 & & \\ & & & 0 & 3\,k_{Ca_o}\,\mathrm{diag}\,(1,\ldots,k-j) & & \\ & & & & & \ddots & \\ & & & & & & 3\,k_{Ca_c} \end{bmatrix}, \tag{30}$$

$$K_{Ca_{2_{n_S\times n_S}}} = \begin{bmatrix} 2\,k_{Ca_c} & 0 & & & & & \\ 0 & 2\,k_{Ca_o}\,\mathrm{diag}\,(1,\ldots,k) & & & & & \\ & & \ddots & & & & \\ & & & 2\,k_{Ca_c} & 0 & & \\ & & & 0 & 2\,k_{Ca_o}\,\mathrm{diag}\,(1,\ldots,k-j) & & \\ & & & & & \ddots & \\ & & & & & & 2\,k_{Ca_c} \end{bmatrix}, \tag{31}$$

$$D_{A_{n_S\times n_S}} = \begin{bmatrix} A_c & 0 & & & & & \\ 0 & A_o\,\mathrm{diag}\,(1,\ldots,k) & & & & & \\ & & \ddots & & & & \\ & & & A_c & 0 & & \\ & & & 0 & A_o\,\mathrm{diag}\,(1,\ldots,k-j) & & \\ & & & & & \ddots & \\ & & & & & & A_c \end{bmatrix}. \tag{32}$$

Then, the expected exocytosis rate for the single granule coupled with k CaVs, λ_{Y_k}, can be estimated by using equation (23), assuming initially the granule in state G_0 and the k CaVs closed, i.e., the complex is initially in state C_kG_0 ($\boldsymbol{\pi} = \left(1, \mathbf{0}_{1\times(3n_S-1)}\right)$, which yields

$$\lambda_{Y_k} = \frac{1}{\boldsymbol{\pi}\left(-{D_{G:kCaV}}^{-1}\right)\mathbf{1}} \tag{33}$$

where $\mathbf{1} \in \mathbb{R}^{3n_S\times 1}$.

For the particular case with non-inactivating CaVs channels, $M_{kCaV} = M_0$ by equations (26) and (27) with $\delta = \gamma = 0$, and then, $D_{G:kCaV}$, given by equation (29), belongs to $\mathbb{R}^{3(k+1)\times 3(k+1)}$.

In order to compare the rate for a granule coupled with different number k of CaVs, we define the relative rate, ρ_{λ_k}, as

$$\rho_{\lambda_k} = \frac{\lambda_{Y_k}}{\lambda_{Y_n}} \tag{34}$$

with $k = 1, \ldots, n$. Moreover, in order to compare the rate at different distances from the granule to CaVs, we define the relative distance rate, ρ_{λ_d}, as

$$\rho_{\lambda_d} = \frac{\lambda_{Y_d}}{\lambda_{Y_{d_{min}}}} \tag{35}$$

where λ_{Y_d} is the rate computed at a given distance r_G and $\lambda_{Y_{d_{min}}}$ the rate computed at $r_G = 10$ nm.

Results and Discussion

We analyze the behavior of the devised exocytosis model where the single granule is coupled with k Ca^{2+} channels by using phase-type distribution results for Markov chains [9] (see Methods). First, we assume that a granule is coupled with one CaV and, then, we extend the results to a more general case with k CaVs. Moreover, we consider for both the cases (1 or k CaVs) that the granule forms complexes with inactivating or non-inactivating CaVs. This scenario reflects e.g. what it is observed in pancreatic beta-cells where the two main high voltage-activated Ca^{2+} channels, the L- and P/Q-type Ca^{2+} channels, are examples of inactivating and non-inactivating CaVs, respectively [20].

Granule coupled with one inactivating (or non-inactivating) CaV

Fig. 2A shows the expected exocytosis rate, λ_{Y_1} computed by equation (25), for a granule at different distances from an inactivating CaV channel. Independently of the distance to the CaV, the exocytosis rate has a bell-shaped relation to voltage, as seen experimentally [21, 22, 20]. The same holds true in the case of non-inactivating CaV (Fig. 2B). As the distance between the granule and the Ca^{2+} channel increases, the expected rate decreases substantially and nonlinearly (for instance, in Fig. 2A, compare the red and blu lines for $r_G = 20$ nm, and $r_G = 10$ nm, respectively). This is clearer from Fig. 2C, showing the relative distance rate ρ_{λ_d} defined by equation (35) for different values of r_G. Note that increasing the distance by a factor of two corresponds to a more than five-fold reduction of the exocytosis rate (the relative ratio is less than 0.2, see the red plot in Fig. 2C). This steep dependence of the distance to the channel is because the calcium levels drop rapidly, moving away from the channel [7, 23].

We perform a similar analysis for the case where a granule is coupled with a non-inactivating CaV (Fig. 2B). We note an increase about of two orders of magnitudes for the exocytosis rate compared to the case with a granule coupled with an inactivating CaV (see Figs. 2A-B): the exocytosis proceeds more rapidly since the triggering Ca^{2+} signal is increased due to non-inactivation of Ca^{2+} currents [24]. Also in this case the degree of decrease for the rate is much higher than the relative increase for the distance (Fig. 2D). However, the benefit in terms of ρ_{λ_d} by reducing the distance is slightly less than that obtained with inactivating CaV (compare Figs. 2C and 2D): for the case with inactivating CaV, it seems that moving away from the channel, ρ_{λ_d} decreases more due to the inactivation of CaV that determines a further drop of calcium levels.

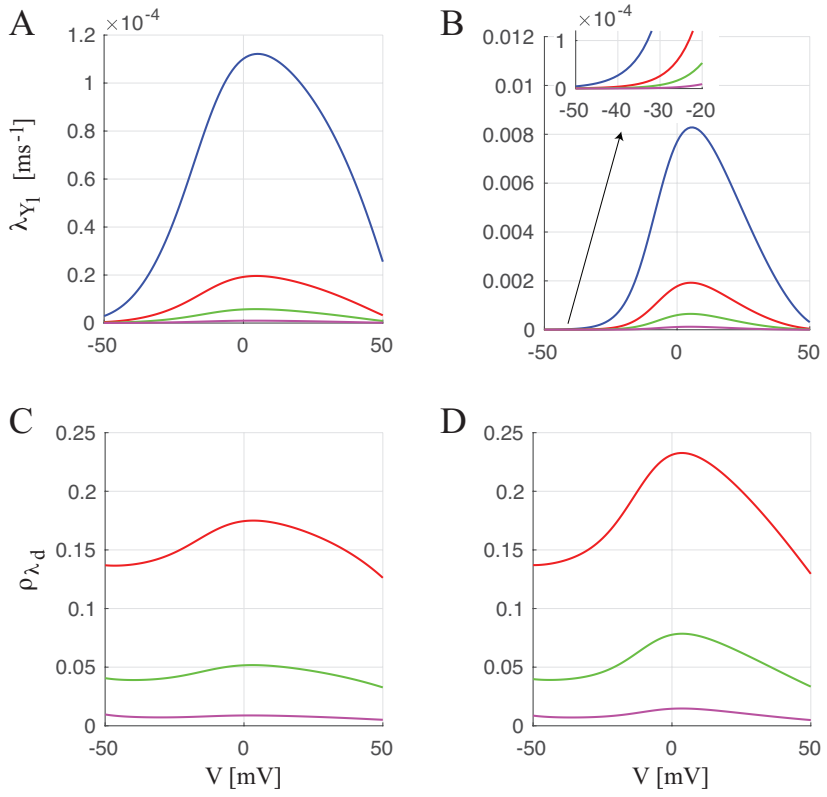

Figure 2: **Expected exocytosis rate for single granule coupled with one (inactivating or non-inactivating) CaV. (A-B)** Expected exocytosis rate λ_{Y_1} for the granule at different distances r_G from one inactivating (A) or non-inactivating (B) CaV: $r_G = 10$ nm (blue curves), $r_G = 20$ nm (red), $r_G = 30$ nm (green) and $r_G = 50$ nm (magenta). Note the different scales on the y-axes. The insert in panel B is a zoom on the lower, left part of the figure for comparison with panel A. **(C-D)** Relative rate ρ_{λ_d} computed at different distances ($r_G = 20$ nm (red), $r_G = 30$ nm (green) and $r_G = 50$ nm (magenta)) of the granule from the inactivating (C) or not-inactivating (D) CaV, and compared to the case with $r_G = 10$ nm.

Granule coupled with k inactivating (or not-inactivating) CaVs

Figs. 3A-D show the expected exocytosis rate λ_{Y_k} computed by equation (33), for a granule coupled with different numbers of inactivating CaVs, and at fixed distances between the granule and the CaVs. It is clear that increasing the number of CaVs coupled with the granule determines a rise of the exocytosis rate. Moreover, as the number of CaVs coupled with the granule increases, the rise in the rate is more pronounced when the distance of the granule from the CaVs is small. This is evident by considering the relative rate ρ_{λ_k} defined by equation (34) (Fig. 3E). For instance, consider the cyan curves computed for $k = 4$ with different types of lines denoting the different distances of the granule from the CaVs. In this case the number of CaVs decreases by a factor of 2 (from 8 to 4) while the exocytosis rate drops more than three fold for $r_G = 20$ nm (dashed cyan line, $\rho_{\lambda_k} < 0.3$, for $V > -10$ mV) and more than five fold for $r_G = 10$ nm (solid cyan line, $\rho_{\lambda_k} < 0.2$, for $V > -10$ mV).

As done for the case with one CaV, we performed the same analysis with k non-inactivating CaVs coupled with the granule (see Figs. 3F-I). Also in this case, it is clear that increasing the number of CaVs determines a rise of the exocytosis rate for the granule. Surprisingly and in contrast with the case with inactivating CaVs, as the number of non-inactivating CaVs increases, the relative rise in exocytosis rate is much higher at larger distances from the CaVs, as shown in Fig. 3J reporting the relative rate ρ_{λ_k}. In case the number of CaVs is reduced from 8 to 4, the exocytosis rate decreases by 2-2.5 fold when the granule is nearby the CaVs (see the solid cyan curve for $r_G = 10$ nm, $0.4 < \rho_{\lambda_k} < 0.5$ with -20 mV $< V < 40$ mV), while it goes down five fold when the granule is far from CaVs (see the dotted cyan curve for $r_G = 50$ nm, $0.2 < \rho_{\lambda_k} < 0.3$ with -20 mV $< V < 40$ mV). It seems that when the granule is surrounded by more non-inactivating CaVs, it is not necessary that the granule is very close to the CaVs for triggering exocytosis.

Relationship between Ca^{2+} influx and exocytosis

To investigate the relationship between exocytosis and Ca^{2+} loading, we consider a set of scenarios where the granule is coupled with different number of non-inactivating or inactivating CaVs, placed very close (10 nm) or far (100 nm) from the granule. Fig. 4A shows the calcium current at $V = 0$ mV, for different numbers of non-inactivating CaVs, while Fig. 4B shows the corresponding cases with inactivating CaVs. In the latter, it is evident how the calcium influx drops after few tens of ms due to the inactivation of the CaVs. Figs. 4C and D show the probability of exocytosis p_Y ($p_Y = P(S(t) = Y)$) vs. the integral of the Ca^{2+} current, Q_{Ca}, defined by equation (9), for the granule placed close to the CaV cluster, for different numbers of CaVs ($r_G = 10$ nm). For the case of non-inactivating CaVs (Fig. 4C), p_Y raises linearly with Q_{Ca}, with slope that increases with the number of CaVs, and then saturates due to the depletion of the granule pool as p_Y approaches 1 (see also ref. [25]). For inactivating CaVs, we note a change of the slope of the linearity between p_Y and Q_{Ca} that is not only due to depletion (when $y \geq 0.5$) but also to near-complete inactivation of CaVs, in particular after 50 ms (Fig. 4D). Figs. 4E and F show p_Y vs. Q_{Ca} when the granule is placed far from CaVs ($r_G = 100$ nm). Due to the distance to CaVs, the calcium concentration at the granule increases only modestly,

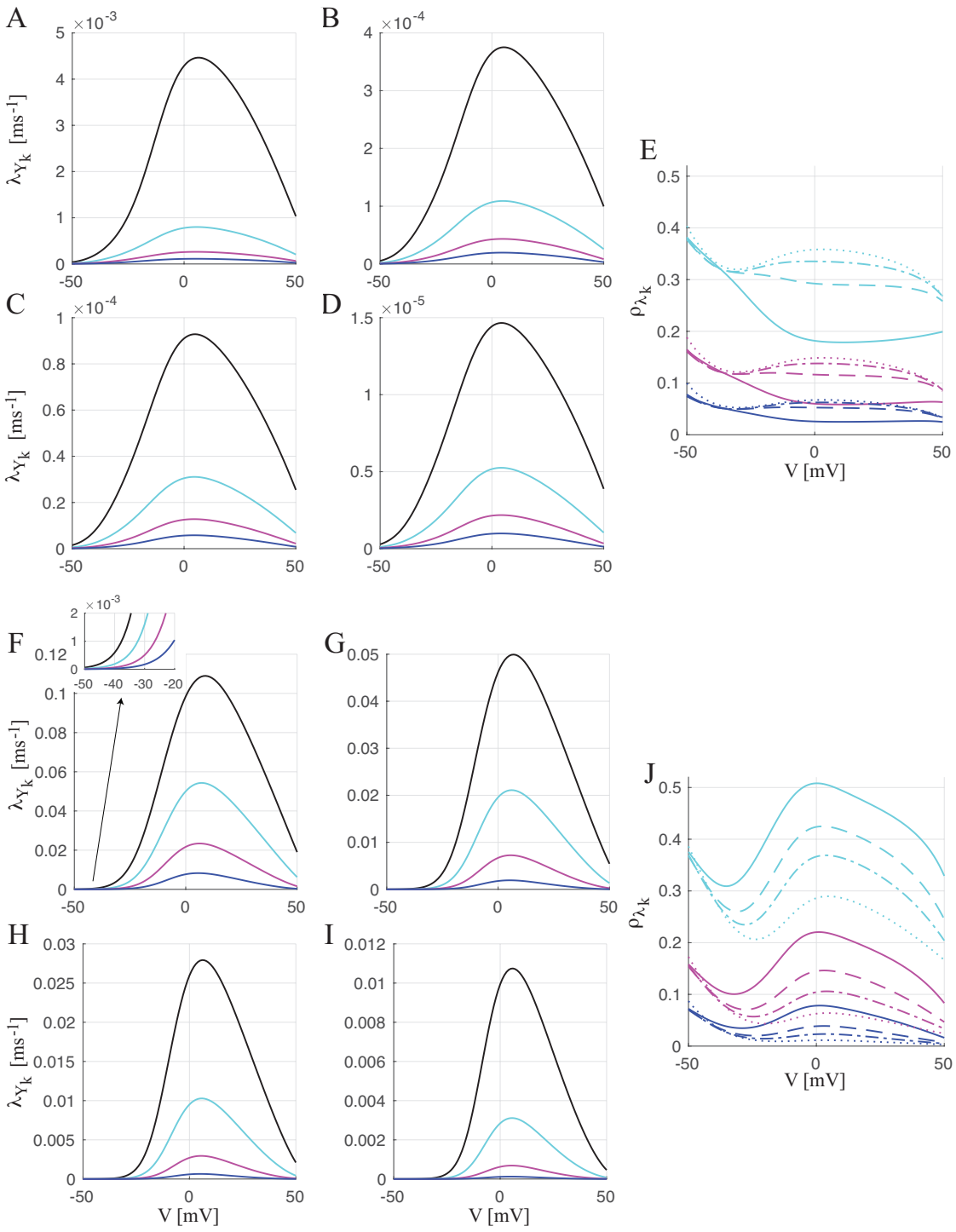

Figure 3: **Expected exocytosis rate for single granule coupled with k (inactivating or non-inactivating) CaVs. (A)-(D), (F)-(I)** Expected exocytosis rate λ_{Y_k} for the granule at fixed distance r_G from k ($k = 1$ (blue curves), $k = 2$ (magenta), $k = 4$ (cyan) and $k = 8$ (black)) inactivating/not-inactivating CaVs: $r_G = 10$ nm (A/F), 20 nm (B/G), 30 nm (C/H), 50 nm (D/I). The insert in panel F is a zoom on the lower, left part of the figure for comparison with panel A. **(E), (J)** Relative rate ρ_{λ_k} obtained from the granule coupled with k inactivating/not-inactivating CaVs (E/J), for $k = 1$ (blue), $k = 2$ (magenta) and $k = 4$ (cyan), and compared to the case with $n = 8$ CaVs. The different type of line corresponds to ρ_{λ_k} computed at fixed distance: $r_G = 10$ nm (solid line), $r_G = 20$ nm (dashed), $r_G = 30$ nm (dash-dotted) and $r_G = 50$ nm (dotted).

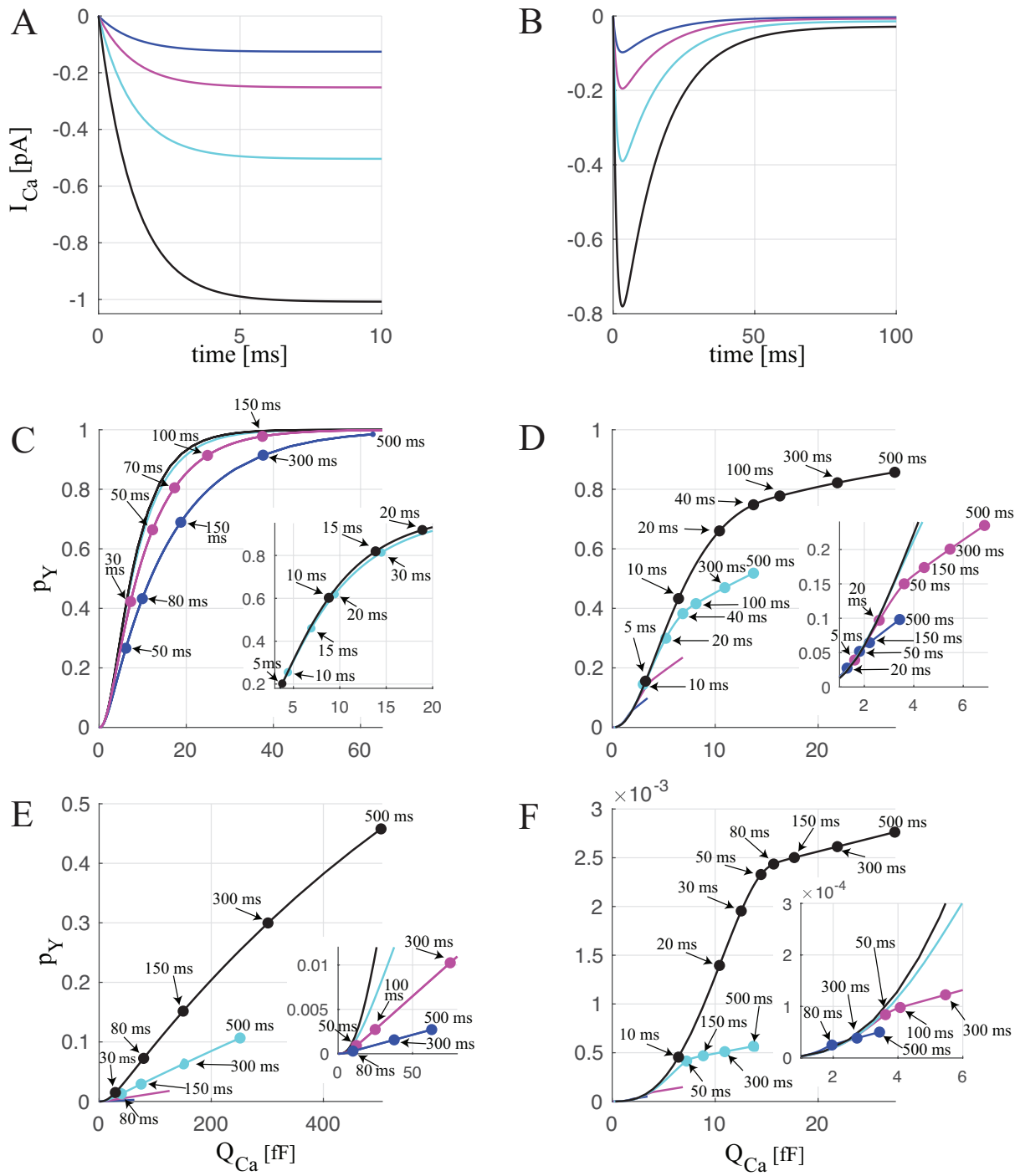

Figure 4: **Relationship between Ca^{2+} influx and exocytosis rate**. **(A, B)** Ca^{2+} current for the different number of non-inactivating (A) and inactivating (B) CaVs. **(C, D)** Probability of exocytosis, p_Y, vs. integral of Ca^{2+} currents, Q_{Ca}, computed at $V = 0$ mV by increasing the integration time, t_s, from 1 to 500 ms, for the granule at distance $r_G = 10$ nm from k not-inactivating (C) or inactivating (D) CaVs. **(E, F)** Legend as in **(C, D)** with $r_G = 100$ nm. In each panel the different colors represent different number of CaVs: blue curve for $k = 1$; magenta for $k = 2$; cyan for $k = 4$; black for $k = 8$. The insets in panels (C–F) show a zoom-in of p_Y vs. Q_{Ca} on lower Q_{Ca} values for the granule coupled with different number k of CaVs: $k = 4$ and 8 in (C), $k = 1$, 2, 4 and 8 in (D–F).

and hence a greater calcium influx Q_{Ca} is needed to allow the granule to move through the Markov Chain from N_0 to Y and undergo exocytosis. This causes an evident initial delay for the granule to be released, resulting in an initial convex relation between p_Y and Q_{Ca}. After this initial phase, for the case of non-inactivating CaVs (Fig. 4E), p_Y raises linearly with Q_{Ca} with slope depending on the number of CaVs. For higher Q_{Ca} the slope of p_Y slightly decreases in the case with $k = 8$ CaVs reflecting slight depletion of the granule pool ($p_Y \approx 0.5$ at $Q_{Ca} = 500$ fF). For inactivating CaVs (Fig. 4F), as for the case with $r_G = 10$ nm, we note a change of the linearity between p_Y and Q_{Ca} that is due to CaV inactivation.

Conclusions

In this paper we devise a strategy that allows us to characterize the local interactions between granules and CaVs. The methodology is similar to our approach for modelling the local effect of CaVs on whole-cell BK currents [8]. We develop Markov chain models describing the dynamics of a single granule coupled with one or more inactivating (or non-inactivating) Ca^{2+} channels, and use phase-type distribution results [9] for estimating the expected exocytosis rate.

We investigate how the release probability of a granule can be affected by varying the number of CaVs and the distance of the (Ca^{2+} sensor of the) granule from CaVs. In particular, from our analysis, we find that the distance between the granule and CaVs is a major factor in determining the exocytosis rate, as we recently demonstrated and quantified explicitly [23]. Further and in agreement with experiments [23], the simulations presented here show that the increase of the number of CaVs coupled with the granule determines a much higher rise of the exocytosis rate, which in the case of inactivating CaVs is more pronounced when the granule is close to CaVs (≈ 10 nm), whereas for non-inactivating CaVs the highest relative increase in rate is obtained when the CaVs are far from CaVs (≈ 50 nm).

We also study the relationship between Ca^{2+} influx and exocytosis. The results of the devised exocytosis model confirm that the granule secretion is generally linearly related to the integral of Ca^{2+}current, as experimentally observed [26, 27, 28, 29, 30, 31] and theoretically justified [25]. Surprisingly, for the case of inactivating CaVs, our analysis shows a change of the linear relation between p_Y and Q_{Ca} due to near-complete inactivation of CaV. This fact is due to the rather complex exocytosis model where the efficacy of Ca^{2+} influx in triggering exocytosis depends on the number of active CaVs, as clearly seen in the case of non-inactivating CaVs (Figs. 4C and 4E), because of multiple steps of Ca^{2+} bindings before exocytosis. During inactivation the effective number of CaVs declines, which has a similar effect as reducing the number of CaVs, and hence the slope of the relation between exocytosis and Q_{Ca} decreases. This finding reinforces the notion that a concave relation between exocytosis and Ca^{2+} influx does not necessarily reflect pool depletion [32] and provide a new example of such as scenario.

Data Availability

No data were used to support this study.

Conflicts of Interest

The authors declare that there is no conflict of interest regarding the publication of this paper.

Funding Statement

F.M. was supported by the University of Padova (Research Grant BIRD 2017).
M.G.P. was supported by the University of Padova (Research Project SID and Research Project PROACTIVE).

References

[1] Robert D. Burgoyne and Alan Morgan. Secretory granule exocytosis. *Physiological Reviews*, 83(2):581–632, apr 2003.

[2] Stanley Misler. Unifying concepts in stimulus-secretion coupling in endocrine cells and some implications for therapeutics. *Advances in Physiology Education*, 33(3):175–186, sep 2009.

[3] S. E. Kahn, S. Zraika, K. M. Utzschneider, and R. L. Hull. The beta cell lesion in type 2 diabetes: there has to be a primary functional abnormality. *Diabetologia*, 52(6):1003–1012, mar 2009.

[4] Frances M. Ashcroft and Patrik Rorsman. Diabetes mellitus and the beta-cell: The last ten years. *Cell*, 148(6):1160–1171, mar 2012.

[5] Sebastian Barg. Mechanisms of exocytosis in insulin-secreting beta-cells and glucagon-secreting alpha-cells. *Pharmacology and Toxicology*, 92(1):3–13, jan 2003.

[6] Francesco Montefusco and Morten Gram Pedersen. Mathematical modelling of local calcium and regulated exocytosis during inhibition and stimulation of glucagon secretion from pancreatic alpha-cells. *The Journal of Physiology*, 593(20):4519–4530, sep 2015.

[7] Erwin Neher. Vesicle pools and Ca^{2+} microdomains: New tools for understanding their roles in neurotransmitter release. *Neuron*, 20(3):389–399, mar 1998.

[8] Francesco Montefusco, Alessia Tagliavini, Marco Ferrante, and Morten Gram Pedersen. Concise whole-cell modeling of BK_{Ca} -CaV activity controlled by local coupling and stoichiometry. *Biophysical Journal*, 112(11):2387–2396, jun 2017.

[9] Peter Buchholz, Jan Kriege, and Iryna Felko. Phase-type distributions. In *Input Modeling with Phase-Type Distributions and Markov Models*, pages 5–28. Springer International Publishing, 2014.

[10] A. Sherman, J. Keizer, and J. Rinzel. Domain model for Ca^{2+}-inactivation of Ca^{2+} channels at low channel density. *Biophysical Journal*, 58(4):985–995, oct 1990.

[11] E. Neher. Concentration profiles of intracellular Ca^{2+} in the presence of diffusible chelator. In *Calcium Electrogenesis and Neuronal Functioning, Exp. Brain Res. 14*, pages 80–96. Springer-Verlag, Berlin, 1986.

[12] Daniel H. Cox. Modeling a Ca^{2+} channel/BK_{Ca} channel complex at the single-complex level. *Biophysical Journal*, 107(12):2797–2814, dec 2014.

[13] Paulo S. Pinheiro, Sébastien Houy, and Jakob B. Sørensen. C2-domain containing calcium sensors in neuroendocrine secretion. *Journal of Neurochemistry*, 139(6):943–958, nov 2016.

[14] Thomas Voets. Dissection of three Ca^{2+} -dependent steps leading to secretion in chromaffin cells from mouse adrenal slices. *Neuron*, 28(2):537–545, nov 2000.

[15] Alessia Tagliavini, Jol Tabak, Richard Bertram, and Morten Gram Pedersen. Is bursting more effective than spiking in evoking pituitary hormone secretion? A spatiotemporal simulation study of calcium and granule dynamics. *American Journal of Physiology-Endocrinology and Metabolism*, 310(7):E515–E525, apr 2016.

[16] Chad P. Grabner, Steven D. Price, Anna Lysakowski, and Aaron P. Fox. Mouse chromaffin cells have two populations of dense core vesicles. *Journal of Neurophysiology*, 94(3):2093–2104, sep 2005.

[17] Sofia A. Andersson, Morten G. Pedersen, Jenny Vikman, and Lena Eliasson. Glucose-dependent docking and SNARE protein-mediated exocytosis in mouse pancreatic alpha-cell. *Pflgers Archiv - European Journal of Physiology*, 462(3):443–454, jun 2011.

[18] Charlotta S. Olofsson, Sven O. Gpel, Sebastian Barg, Juris Galvanovskis, Xiaosong Ma, Albert Salehi, Patrik Rorsman, and Lena Eliasson. Fast insulin secretion reflects exocytosis of docked granules in mouse pancreatic b-cells. *Pflgers Archiv*, 444(1-2):43–51, may 2002.

[19] P M Dean. Ultrastructural morphometry of the pancreatic beta-cell. *Diabetologia*, 9:115–119, April 1973.

[20] M. Braun, R. Ramracheya, M. Bengtsson, Q. Zhang, J. Karanauskaite, C. Partridge, P. R. Johnson, and P. Rorsman. Voltage-gated ion channels in human pancreatic beta-cells: Electrophysiological characterization and role in insulin secretion. *Diabetes*, 57(6):1618–1628, apr 2008.

[21] K D Gillis, R Y Pun, and S Misler. Single cell assay of exocytosis from adrenal chromaffin cells using "perforated patch recording". *Pflugers Archiv : European journal of physiology*, 418:611–613, July 1991.

[22] K L Engisch and M C Nowycky. Calcium dependence of large dense-cored vesicle exocytosis evoked by calcium influx in bovine adrenal chromaffin cells. *The Journal of neuroscience: the official journal of the Society for Neuroscience*, 16:1359–1369, February 1996.

[23] Nikhil R. Gandasi, Peng Yin, Michela Riz, Margarita V. Chibalina, Giuliana Cortese, Per-Eric Lund, Victor Matveev, Patrik Rorsman, Arthur Sherman, Morten G. Pedersen, and Sebastian Barg. Ca^{2+} channel clustering with insulin-containing granules is disturbed in type 2 diabetes. *Journal of Clinical Investigation*, 127(6):2353–2364, may 2017.

[24] Morten Gram Pedersen, Alessia Tagliavini, Giuliana Cortese, Michela Riz, and Francesco Montefusco. Recent advances in mathematical modeling and statistical analysis of exocytosis in endocrine cells. *Mathematical Biosciences*, 283:60–70, jan 2017.

[25] Morten Gram Pedersen. On depolarization-evoked exocytosis as a function of calcium entry: Possibilities and pitfalls. *Biophysical Journal*, 101(4):793–802, aug 2011.

[26] Tobias Moser and Erwin Neher. Rapid exocytosis in single chromaffin cells recorded from mouse adrenal slices. *The Journal of Neuroscience*, 17(7):2314–2323, apr 1997.

[27] S Barg, X Ma, L Eliasson, J Galvanovskis, S O Gpel, S Obermller, J Platzer, E Renstrm, M Trus, D Atlas, J Striessnig, and P Rorsman. Fast exocytosis with few Ca^{2+} channels in insulin-secreting mouse pancreatic beta-cells. *Biophysical journal*, 81:3308–3323, December 2001.

[28] Yang Z. De Marinis, Albert Salehi, Caroline E. Ward, Quan Zhang, Fernando Abdulkader, Martin Bengtsson, Orit Braha, Matthias Braun, Reshma Ramracheya, Stefan Amisten, Abdella M. Habib, Yusuke Moritoh, Enming Zhang, Frank Reimann, Anders H. Rosengren, Tadao Shibasaki, Fiona Gribble, Erik Renstrm, Susumu Seino, Lena Eliasson, and Patrik Rorsman. GLP-1 inhibits and adrenaline stimulates glucagon release by differential modulation of N- and L-type Ca^{2+} channel-dependent exocytosis. *Cell Metabolism*, 11(6):543–553, jun 2010.

[29] Ramachandran Thiagarajan, Jennifer Wilhelm, Teclemichael Tewolde, Yingjie Li, Mark M. Rich, and Kathrin L. Engisch. Enhancement of asynchronous and train-evoked exocytosis in bovine adrenal chromaffin cells infected with a replication deficient adenovirus. *Journal of Neurophysiology*, 94(5):3278–3291, nov 2005.

[30] Morten Gram Pedersen, Giuliana Cortese, and Lena Eliasson. Mathematical modeling and statistical analysis of calcium-regulated insulin granule exocytosis in beta-cells from mice and humans. *Progress in Biophysics and Molecular Biology*, 107(2):257–264, nov 2011.

[31] Morten Gram Pedersen, Vishal Ashok Salunkhe, Emma Svedin, Anna Edlund, and Lena Eliasson. Calcium current inactivation rather than pool depletion explains reduced exocytotic rate with prolonged stimulation in insulin-secreting INS-1 832/13 cells. *PLoS ONE*, 9(8):e103874, aug 2014.

[32] Morten Gram Pedersen. Insulin secretory granules enter a highly calcium-sensitive state following palmitate-induced dissociation from calcium channels: A theoretical study. *Journal of Neuroendocrinology*, 22(12):1315–1324, nov 2010.